

# Dynamical Phase Transitions in a 2D Classical Nonequilibrium Model via 2D Tensor Networks

Phillip Helms\* and Garnet Kin-Lic Chan†

Division of Chemistry and Chemical Engineering, California Institute of Technology, Pasadena, CA 91125

(Dated: June 16, 2022)

We demonstrate the power of 2D tensor networks for obtaining large deviation functions of dynamical observables in a classical nonequilibrium setting. Using these methods, we analyze the previously unstudied dynamical phase behavior of the fully 2D asymmetric simple exclusion process with biases in both the  $x$  and  $y$  directions. We identify a dynamical phase transition, from a jammed to a flowing phase, and characterize the phases and the transition, with an estimate of the critical point and exponents.

**Introduction** – Large deviation theory (LDT) has emerged as a powerful framework for studying the fluctuations of macroscopic dynamical observables in classical nonequilibrium systems [1–5]. Reminiscent of equilibrium statistical mechanics, where ensembles of configurations are organized by their macroscopic properties, such as temperature or energy, LDT prescribes the grouping of trajectories into ensembles based on their dynamical or static macroscopic properties, such as the current or density. This approach allows for the definition of dynamical partition functions, derivatives of which are the mathematical analogs to entropy and free energy, named large deviation functions (LDFs), which encode the statistics of dynamical observable fluctuations. As in equilibrium systems, these are critical for identifying and characterizing phase transitions, particularly those which occur in the space of trajectories, called dynamical phase transitions (DPTs) [5].

The success of LDT has been accompanied by the development of numerical methods for computing LDFs, with significant emphasis and progress centered in sophisticated sampling techniques [4, 6–12]. Alternatively, the matrix product ansatz, a powerful analytical representation of nonequilibrium steady states [13–15], foreshadowed the recent success of numerical tensor network (TN) algorithms. In particular, calculations using matrix product states (MPS), the 1D TN that underpins the density matrix renormalization group (DMRG) algorithm [16], provide a noiseless alternative to sampling methods. As demonstrated in the recent applications to DPTs in kinetically constrained and driven diffusive models [17–21], MPS provide remarkably compact representations of nonequilibrium steady states.

While the TN approach is promising, the use of MPS, which only efficiently encode correlations in one-dimension, limits the study of higher dimensional problems [22]. Consequently, LDF computations beyond one dimension have relied on Monte Carlo methods [23–26]. In this letter, we demonstrate how an inherently 2D TN, the projected entangled pair state (PEPS) [27–30], serves as an efficient ansatz to determine LDFs in 2D nonequilibrium lattice problems. We use this approach to study the dynamical phase diagram of the fully 2D ASEP, an extension of the 1D paradigmatic model of nonequilibrium behavior that still remains poorly characterized [31–36], finding a new DPT between the jammed and flowing phases.

## Large Deviation Theory and Projected Entangled Pair States

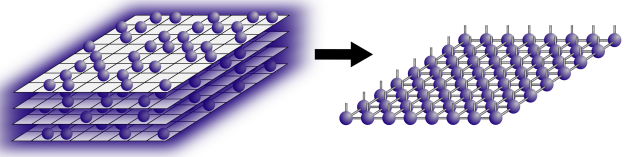


FIG. 1. A stack of possible configurations of the 2D ASEP (left), representing all possible configuration probabilities, is stored as a 2D PEPS, whose TN diagram is shown on the right.

– We begin with a short overview of relevant theory and methods associated with LDT, TNs, and PEPS. More comprehensive treatments of all three topics are provided in recent reviews and methodological papers [5, 28, 30].

A Markovian nonequilibrium system’s time evolution is governed by a master equation,  $\partial_t |P_t\rangle = \mathcal{W}|P_t\rangle$ , where vector  $|P_t\rangle$  represents the configurational probabilities at time  $t$  and the generator,  $\mathcal{W}$ , dictates the transition rates between configurations. At steady-state, the time-averaged current vector,  $\bar{\mathbf{J}} = \mathbf{J}/t$  obeys a large deviation principle,  $P(\bar{\mathbf{J}}) \approx e^{-t\phi(\bar{\mathbf{J}})}$ , as does its moment generating function,  $Z(\lambda) = \langle e^{-\lambda\bar{\mathbf{J}}}\rangle \approx e^{-t\psi(\lambda)}$ , indicating that the probability of observing all but the most likely current decays exponentially with averaging time. The rate function (RF),  $\phi(\bar{\mathbf{J}})$ , defines the probability of a given current, and  $\psi(\lambda)$  is the scaled cumulant generating function (SCGF), whose derivatives at  $\lambda = 0$  give the cumulants of the current.

Performing a tilting of the generator,  $\mathcal{W} \rightarrow \mathcal{W}^{(\lambda)}$ , effectively weights trajectories according to their currents, by scaling all forward (backward) hopping terms by  $e^{-\lambda}$  ( $e^{\lambda}$ ), making  $\mathcal{W}^{(\lambda)}$  non-Markovian and non-Hermitian. A central finding in LDT dictates that the largest eigenvalue of the tilted generator is the SCGF, i.e.  $\mathcal{W}^{(\lambda)}|P^{(\lambda)}\rangle = \psi(\lambda)|P^{(\lambda)}\rangle$ . Furthermore, the corresponding left and right eigenvectors detail trajectory characteristics associated with particular fluctuations. For example, the time averaged local density associated with a fluctuation is  $\rho_i = \langle P^{(\lambda)}|n_i|P^{(\lambda)}\rangle/\langle P^{(\lambda)}|P^{(\lambda)}\rangle$ , where  $n_i$  is the particle number operator and  $\langle P^{(\lambda)}|$  and  $|P^{(\lambda)}\rangle$  are the left and right eigenvectors.

The TN approach provides an intuitive ansatz to directly approximate the eigenstates of the tilted generator. A tensor is allocated for each lattice site; one index of this tensor specifies the state of the local site (i.e. empty or occupied), while

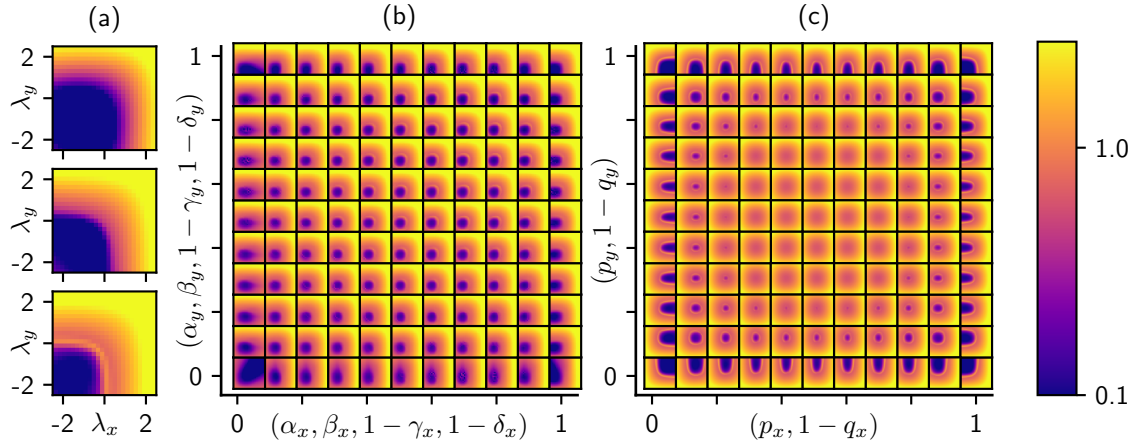


FIG. 2. A mapping of the mean field dynamical phase diagram of the 2D ASEP with (a) showing the SCGF, current, and current susceptibility as a function of bias at one point in the physical phase space, while (b) and (c) respectively show plots of the current susceptibility as a function of bias for a bulk biased and a boundary biased 2D ASEP. For (a),  $p_{x,y} = 1 - q_{x,y} = 1$  with boundary terms at  $1/2$  and current biases,  $\lambda_x, \lambda_y \in [-2.5, 2.5]$ ; we can see the transition between the jammed (dark) and flowing (bright) phases. In (b), bulk rates are fixed at  $p_{x,y} = 1 - q_{x,y} = 0.9$  while sweeping over a subset of boundary rates ( $\alpha_{x,y} = \beta_{x,y} = 1 - \gamma_{x,y} = 1 - \delta_{x,y}$ ). In (c), all boundary terms are set to  $1/2$  and we sweep over bulk hopping rates ( $p_{x,y}, q_{x,y}$ ). Each subplot in (b) and (c) sweeps over current biases  $\lambda_x, \lambda_y \in [-2.5, 2.5]$ .

additional indices connect nearest neighboring sites, resulting in, for example, rank five bulk tensors for a square lattice. The connecting indices enable information transfer between sites, and their size, termed the bond dimension  $D$ , controls the effective Hilbert space of the ansatz, which becomes exact for sufficiently large  $D$ . The resulting network of tensors is shown on the right of Figure 1, emphasizing how the probabilities of all steady state system configurations (left) are stored as a single PEPS (right).

The development of appropriate PEPS optimization techniques for quantum many body problems is an active area of research [37–40]. For this work, we simply adopt many of the most successful standard techniques. Using the time-evolving block decimation approach [28, 41], we integrate the tilted master equation forwards in time, giving  $|P_t^{(\lambda)}\rangle = e^{t\mathcal{W}^{(\lambda)}}|P_0^{(\lambda)}\rangle$ . We apply the time evolution operator to the initial PEPS via its Suzuki-Trotter decomposition into local gates,  $e^{t\mathcal{W}^{(\lambda)}} \approx \left(e^{\delta t \mathcal{W}_{i,i+1}^{(\lambda)}}\right)^{t/\delta t}$ , and iterate this application until convergence to the steady-state. The bond dimension between two sites grows after the application of the gate, thus an alternating least squares approach is used to compress the tensors back to dimension  $D$  [30]. The alternating least squares algorithm uses information from all the other tensors which are contracted into an approximate environment using the single-layer boundary method [42] and tensor reduction [43, 44]. The accuracy of the environment is then determined by an additional parameter,  $\chi$ , which corresponds to the bond dimension of a boundary MPS. Like  $D$ ,  $\chi$  must also be increased to converge to the exact stationary state. In practice, because the environment computation is expensive, we first determine an approximate stationary state via the “simple update” algorithm

where no environment is used [45]; then  $D$  and  $\chi$  are increased in subsequent time evolution steps using the full environment information (“full update” algorithm [41]) while  $\delta t$  is also decreased to reduce the Suzuki-Trotter error.

**Model: 2D ASEP** – The 2D ASEP, Figure 1 (left), takes place on a square  $N \times N$  lattice, where each site may be occupied by a particle or empty. Particles stochastically hop into vacant nearest-neighbor lattice sites in the right (up) and left (down) directions at rates  $p_x$  ( $p_y$ ) and  $q_x$  ( $q_y$ ) respectively. At the {left, bottom, right, top} boundaries, particles are inserted at rates  $\{\alpha_x, \alpha_y, \delta_x, \delta_y\}$ , and removed at rates  $\{\gamma_x, \gamma_y, \beta_x, \beta_y\}$ . Additionally, as detailed in the previous section, we utilize a current bias in both directions,  $\lambda = (\lambda_x, \lambda_y)$ , to probe the trajectory phase space. The tilted generator is built from hopping operators  $\hat{o}_{i,j}^{\text{hop}} = r_{i,j}(e^{\lambda_{i,j}} \mathbf{a}_i \mathbf{a}_j^\dagger - \mathbf{n}_i \mathbf{v}_j)$  and similarly defined insertion and removal operators, where  $r_{i,j}$  is the hopping rate from site  $i$  to  $j$  and  $\mathbf{a}_i, \mathbf{a}_i^\dagger, \mathbf{n}_i$ , and  $\mathbf{v}_i$  are respectively annihilation, creation, particle number and vacancy operators. Because hopping occurs only between nearest neighbor sites, the full tilted generator,  $\mathcal{W}^{(\lambda)}$ , then decomposes naturally into nearest neighbor gates. At  $\lambda_{i,j} = 0, \forall(i, j)$ , the system undergoes its typical dynamics, otherwise the biasing allows for probing of rare trajectories.

**Results** – We first probed for the existence of a DPT in the 2D ASEP by performing mean field (MF) computations of the SCGF in two subsets of the phase space, with results shown in Figure 2. In Figure 2(a) we show, from top to bottom, the per site SCGF, current, and current susceptibility at  $p_{x,y} = 1 - q_{x,y} = 1$  with  $\alpha_{x,y} = \beta_{x,y} = \gamma_{x,y} = \delta_{x,y} = 1/2$  and current biases sweeping over  $\lambda_x, \lambda_y \in [-2.5, 2.5]$ . In the bottom left of these plots, we see a low current regime materialize, bounded by a small peak in

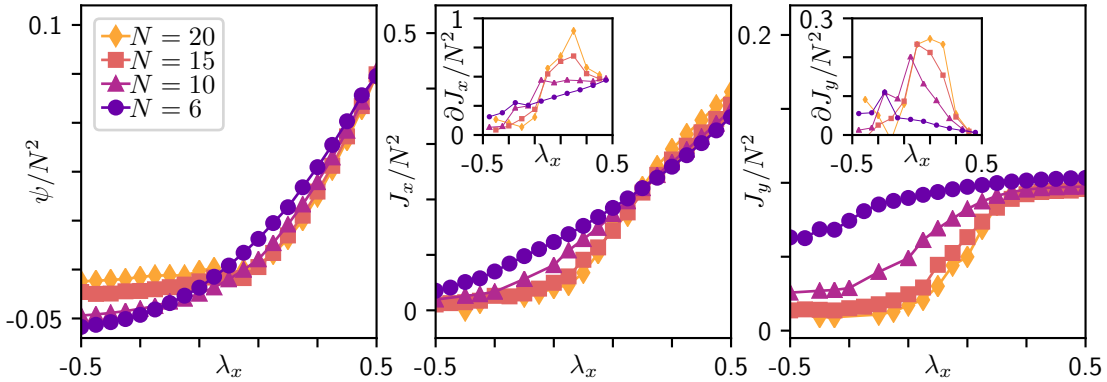


FIG. 3. PEPS calculation results analyzing the phase transition along a line in the dynamical phase space of the 2D ASEP. From left to right, we show the per site SCGF  $\psi(\lambda_x, \lambda_y)/N^2$ , horizontal current  $J_x/N^2$ , and vertical current  $J_y/N^2$  at  $\lambda_y = -1/2$  with  $\lambda_x \in [-1/2, 1]$ . The insets show the derivative of the per site horizontal and vertical currents with respect to  $\lambda_x$ , both of which serve as indicators of the DPT. Each line corresponds to a system size  $N \in [6, 10, 15, 20]$ .

the susceptibility (the thin bright line between the purple and orange regions).

To further explore the phase space, Figure 2 (b) and (c) contain subplots at various points in the rate parameter space, each showing the per site current susceptibility as a function of  $\lambda_{x,y} \in [-2.5, 2.5]$ . (a) explores boundary effects, sweeping boundary terms with  $\alpha_{x,y} = \beta_{x,y} = 1 - \gamma_{x,y} = 1 - \delta_{x,y}$  and maintaining asymmetric interior rates  $p_{x,y} = 1 - q_{x,y} = 0.9$  while (b) probes the effect of bulk hopping rates, sweeping interior hopping rates while holding boundary terms at  $\alpha_{x,y} = \beta_{x,y} = \gamma_{x,y} = \delta_{x,y} = 1/2$ .

We would expect a phase transition to be marked by a peak in current susceptibility, as seen in Figure 2 (a). In Figure 2 (c) this becomes visible at sufficiently high biases ( $\approx p_x > 0.8$ ), again accompanied by a region of distinctly low current. This aligns with the known behavior of the 1D ASEP, where a DPT is observed except when  $p_x = q_x = 1/2$ , which corresponds to the Symmetric Simple Exclusion Process (SSEP). Furthermore, intuition from the 1D ASEP would further predict a DPT to appear for low biases in the thermodynamic limit. For the boundary biased results, Figure 2 (b), we observe the boundary rates to have little effect, except at extreme values, where the location of the DPT becomes distorted due to no insertion or removal at a boundary.

Selecting a line within the phase space covered in Figure 2 (c) at  $p_{x,y} = 1 - q_{x,y} = 0.9$  and  $\lambda_y = -1/2$  with  $\lambda_x \in [-1/2, 1/2]$ , we carried out PEPS calculations on  $N \times N$  lattices with  $N \in \{6, 10, 15, 20\}$ ,  $D \in [2, 8]$  and  $\chi \in [10, 50]$ , while systematically reducing  $\delta t \in [10^{-1}, 10^{-3}]$ . Figure 3 displays key results from these calculations.

There, the left plot shows the SCGF for the  $\lambda_x$  sweep, with the flattening of the curve at  $\lambda < 0$  indicating a low current region. The horizontal and vertical currents were measured via corresponding operators contracted with the left and right PEPS eigenstates of  $\mathcal{W}^{(\lambda)}$  and are shown in the center and right plots of Figure 3. The insets in these plots further show nu-

merical derivatives of the currents with respect to  $\lambda_x$ , which serves as an indicator of the sharpness of the transition, with the derivative of the horizontal current also being the horizontal current susceptibility. In all plots, we see two distinct regions of behaviour, indicative of a DPT. Moving from right to left, we see the emergence of a low current phase, to the left of  $\lambda_x = 1/4$ , where little current flows in either direction. The transition becomes sharper as the size of the lattice increases, as seen by the increasing peaks in current susceptibility, substantiating the existence of a second order DPT between the jammed and flowing phases. The density of the lattices in these phases further reveals configurational differences, where the flowing phase gives the bulk time-averaged site density at half-filling particles are spaced evenly to allow maximal hopping. The jammed phase, alternatively indicates the lattice is entirely filled, with bulk density  $\rho_{bulk} \approx 1$ , preventing any flow away from the boundaries.

To gauge the accuracy of these results, Figure 4 displays the convergence of observables for calculations with  $N = 6$ . Here, relative errors in the SCGF, computed from the right and left eigenstates,  $\psi$  and  $\psi_l$ , and the horizontal and vertical currents,  $J_x$  and  $J_y$ , are computed, using the most accurate available results, with  $(D, \chi, \delta t) = (8, 60, 10^{-3})$ , as a reference and averaged over many results at  $\lambda_y = -1/2$  with  $\lambda_x < 0$  (top) and  $\lambda_x > 0$  (bottom), roughly corresponding to the jammed and flowing phases. Shaded regions correspond to  $D$ , increasing from left to right, where within each shaded region, the accuracy is improved by growing  $\chi$  and shrinking  $\delta t$ .

We find that calculations in the flowing phase converge more easily than those in the jammed phase. Two likely reasons for convergence difficulties in this region exist. First, the jammed nature of the state causes slow dynamics, meaning long evolutions at small time steps are required for better convergence. Second, as seen in the 1D ASEP [21], we observe degenerate ground states in this regime of the 2D ASEP, which was determined via state averaged DMRG calculations. Also,

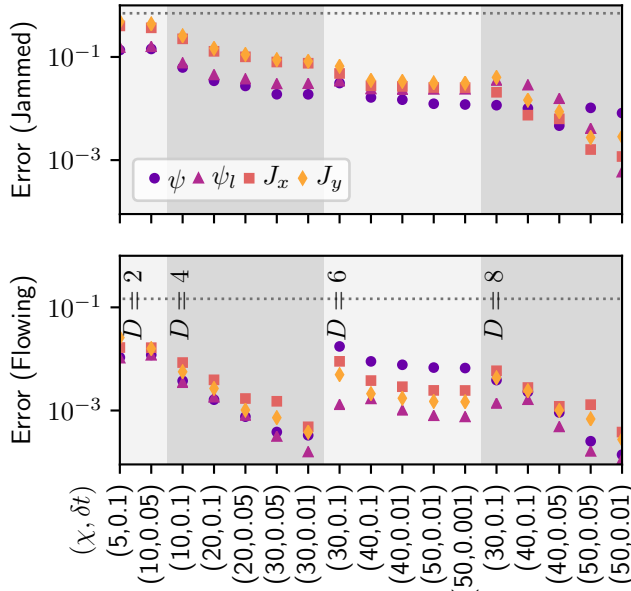


FIG. 4. The convergence of PEPS calculations, showing relative errors for the SCGF,  $\psi$  and  $\psi_l$ , calculated from the left and right eigenstates, vertical current,  $J_y$ , and horizontal current,  $J_x$ . These are shown as a function of bond dimension (shaded), the boundary  $\chi$  dimension  $\chi$  and time step size  $\delta t$  (labeled as  $(\chi, \delta t)$  along the  $x$ -axis) for a  $6 \times 6$  lattice. The top (bottom) plot corresponds to an error averaged over calculations in the jammed (flowing) phase at  $\lambda_x < 0$  ( $\lambda_x > 0$ ). The grey dashed line shows the error of mean-field calculations for reference.

the  $D = 4$  calculations appear to converge more fully than those with  $D = 6$ , which highlights the lack of a variational principle, meaning the SCGF may fluctuate above and below its accurate value. Promisingly, we find a significant increase in accuracy when compared to MF results and easily obtain two to three digits of accuracy for moderate computations, comparable to what is obtained via conventional methods.

Last, we can perform a finite size scaling analysis of the observed transition to extract the critical exponents in the thermodynamic limit. Assuming the scaling relation for the per site horizontal current to be  $j_x(\lambda_x^*, N) = N^d f(\lambda_x^* N^c)$ , where  $d$  and  $c$  are critical exponents,  $f$  is the scaling function, and  $\lambda_x^*$  is analogous to a reduced temperature, i.e.  $\lambda_x^* = (\lambda - \lambda_c)/\lambda_c$ . The critical parameters can then be computed via numerical data collapse [46], giving  $d = -2.25 \pm 0.1$ ,  $c = 0.58 \pm 0.1$ , and  $\lambda_c = 0.41 \pm 0.1$ , with Figure 5 showing the resulting scaling plot, which displays good data collapse. Additionally, the inset of Figure 5 shows that a simple linear extrapolation of  $\lambda_c(N)$ , determined by the location of the susceptibility peak, agrees with the numerically optimized  $\lambda_c$  obtained by the scaling analysis.

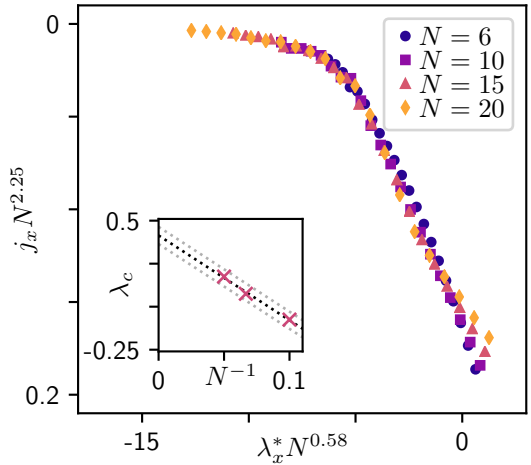


FIG. 5. Scaling plot of the transition between the flowing and jammed phases, showing the collapse of the per site horizontal current as a function of the reduced horizontal bias,  $\lambda_x^*$ . The inset plot shows another estimate of the critical point  $\lim_{N \rightarrow \infty} \lambda_c = 0.41 \pm 0.1$ , with  $\lambda_c(N)$  determined from the location of the susceptibility peak in Figure 3, and with approximate errors from the spacing of points in the susceptibility calculation. The two estimates of the critical point agree up to error bars.

**Conclusions** – We have provided the first insights into the dynamical phase behavior of the fully 2D ASEP, finding evidence for a dynamical phase transition between a flowing and a jammed phase, as detected by a sharp change in the current in the horizontal or vertical direction. We have also demonstrated how 2D tensor networks, in particular the PEPS ansatz, can be used to compute large deviation functions in classical nonequilibrium systems, characterize nonequilibrium phases, and obtain critical exponents. This is a natural extension of the success of 1D tensor network methods in this field and provides significant promise for the future use of TNs in coordination with LDT. Because numerical methods based on PEPS are relatively young, continued progress is likely, and we expect such higher dimensional TNs to become standard tools in the study of nonequilibrium classical statistical mechanics.

**Acknowledgments** – This work was supported primarily by the US National Science Foundation via award no. 1665333. PH was also supported by a NSF Graduate Research Fellowship under grant DGE-1745301 and an ARCS Foundation Award.

\* phelms@caltech.edu

† garnetc@caltech.edu

[1] B. Derrida, Journal of Statistical Mechanics: Theory and Experiment **2007**, P07023 (2007).

- [2] J. P. Garrahan, R. L. Jack, V. Lecomte, E. Pitard, K. van Duijvendijk, and F. van Wijland, *Journal of Physics A: Mathematical and Theoretical* **42**, 075007 (2009).
- [3] A. Prados, A. Lasanta, and P. I. Hurtado, *Physical review letters* **107**, 140601 (2011).
- [4] U. Ray, G. K.-L. Chan, and D. T. Limmer, *The Journal of chemical physics* **148**, 124120 (2018).
- [5] H. Touchette, *Physics Reports* **478**, 1 (2009).
- [6] U. Ray, G. K.-L. Chan, and D. T. Limmer, *Physical review letters* **120**, 210602 (2018).
- [7] T. Nemoto, F. Bouchet, R. L. Jack, and V. Lecomte, *Physical Review E* **93**, 062123 (2016).
- [8] K. Klymko, P. L. Geissler, J. P. Garrahan, and S. Whitelam, *Physical Review E* **97**, 032123 (2018).
- [9] T. Nemoto, R. L. Jack, and V. Lecomte, *Physical review letters* **118**, 115702 (2017).
- [10] U. Ray and G. K. Chan, arXiv preprint arXiv:1909.11283 (2019).
- [11] G. Margazoglou, L. Biferale, R. Grauer, K. Jansen, D. Mesterházy, T. Rosenow, and R. Tripiccione, *Physical Review E* **99**, 053303 (2019).
- [12] A. Das and D. T. Limmer, *The Journal of Chemical Physics* **151**, 244123 (2019).
- [13] R. A. Blythe and M. R. Evans, *Journal of Physics A: Mathematical and Theoretical* **40**, R333 (2007).
- [14] S. Prolhac, M. R. Evans, and K. Mallick, *Journal of Physics A: Mathematical and Theoretical* **42**, 165004 (2009).
- [15] B. Derrida, M. R. Evans, V. Hakim, and V. Pasquier, *Journal of Physics A: Mathematical and General* **26**, 1493 (1993).
- [16] U. Schollwöck, *Annals of Physics* **326**, 96 (2011).
- [17] M. Gorissen, A. Lazarescu, K. Mallick, and C. Vanderzande, *Physical review letters* **109**, 170601 (2012).
- [18] M. Gorissen and C. Vanderzande, *Journal of Physics A: Mathematical and Theoretical* **44**, 115005 (2011).
- [19] M. Gorissen, J. Hooyberghs, and C. Vanderzande, *Physical Review E* **79**, 020101 (2009).
- [20] M. C. Bañuls and J. P. Garrahan, arXiv preprint arXiv:1903.01570 (2019).
- [21] P. Helms, U. Ray, and G. K.-L. Chan, *Phys. Rev. E* **100**, 022101 (2019).
- [22] E. M. Stoudenmire and S. R. White, *Annu. Rev. Condens. Matter Phys.* **3**, 111 (2012).
- [23] N. Tizón-Escamilla, C. Pérez-Espigares, P. L. Garrido, and P. I. Hurtado, *Physical review letters* **119**, 090602 (2017).
- [24] J. P. Garrahan, R. L. Jack, V. Lecomte, E. Pitard, K. van Duijvendijk, and F. van Wijland, *Physical review letters* **98**, 195702 (2007).
- [25] L. O. Hedges, R. L. Jack, J. P. Garrahan, and D. Chandler, *Science* **323**, 1309 (2009).
- [26] D. Chandler and J. P. Garrahan, *Annual review of physical chemistry* **61**, 191 (2010).
- [27] F. Verstraete, M. M. Wolf, D. Perez-Garcia, and J. I. Cirac, *Physical review letters* **96**, 220601 (2006).
- [28] M. Lubasch, J. I. Cirac, and M.-C. Banuls, *New Journal of Physics* **16**, 033014 (2014).
- [29] R. Orús, *Annals of Physics* **349**, 117 (2014).
- [30] H. N. Phien, J. A. Bengua, H. D. Tuan, P. Corboz, and R. Orús, *Physical Review B* **92**, 035142 (2015).
- [31] F. J. Alexander, Z. Cheng, S. A. Janowsky, and J. L. Lebowitz, *Journal of statistical physics* **68**, 761 (1992).
- [32] Z.-J. Ding, S.-L. Yu, K. Zhu, J.-X. Ding, B. Chen, Q. Shi, X.-S. Lu, R. Jiang, and B.-H. Wang, *Physica A: Statistical Mechanics and its Applications* **492**, 1700 (2018).
- [33] N. Singh and S. M. Bhattacharjee, *Physics Letters A* **373**, 3113 (2009).
- [34] H.-T. Yau, *Annals of mathematics* , 377 (2004).
- [35] M. Tamm, S. Nechaev, and S. N. Majumdar, *Journal of Physics A: Mathematical and Theoretical* **44**, 012002 (2010).
- [36] B. Schmittmann, K. Hwang, and R. Zia, *EPL (Europhysics Letters)* **19**, 19 (1992).
- [37] P. Corboz, *Physical Review B* **94**, 035133 (2016).
- [38] L. Vanderstraeten, J. Haegeman, and F. Verstraete, *Physical Review B* **99**, 165121 (2019).
- [39] M. J. O'Rourke and G. K. Chan, arXiv preprint arXiv:1911.04592 (2019).
- [40] R. Haghshenas, M. J. O'Rourke, and G. K.-L. Chan, *Physical Review B* **100**, 054404 (2019).
- [41] M. Lubasch, J. I. Cirac, and M.-C. Banuls, *Physical Review B* **90**, 064425 (2014).
- [42] Z. Y. Xie, H. J. Liao, R. Z. Huang, H. D. Xie, J. Chen, Z. Y. Liu, and T. Xiang, *Phys. Rev. B* **96**, 045128 (2017).
- [43] P. Corboz, R. Orús, B. Bauer, and G. Vidal, *Phys. Rev. B* **81**, 165104 (2010).
- [44] C. Pineda, T. Barthel, and J. Eisert, *Phys. Rev. A* **81**, 050303 (2010).
- [45] H.-C. Jiang, Z.-Y. Weng, and T. Xiang, *Physical review letters* **101**, 090603 (2008).
- [46] S. M. Bhattacharjee and F. Seno, *Journal of Physics A: Mathematical and General* **34**, 6375 (2001).